Electrochemical Engineering
https://www.sciltp.com/journals/ee

Article

Development of $AgBiS_2$ Nanoparticle Modified Bulk Screen-Printed Electrodes for Lead (II) and Cadmium (II) Detection

Enyioma C. Okpara [1,2,*], Timothy O. Ajiboye [3,4], Olanrewaju B. Wojuola [1], Damian C. Onwudiwe [4,5], Elena Bernalte [2], Robert D. Crapnell [2], Matthew J. Whittingham [2] and Craig E. Banks [2]

[1] Department of Physics, Faculty of Natural and Agricultural Science, North-West University (Mafikeng Campus), Private Bag, X2046, Mmabatho 2735, South Africa
[2] Faculty of Science and Engineering, Manchester Metropolitan University, Chester Street, Manchester M1 5GD, UK
[3] Chemistry Department, Nelson Mandela University, University Way, Summerstrand, Gqeberha 6031, South Africa
[4] Material Science Innovation and Modelling (MaSIM) Research Focus Area, Faculty of Natural and Agricultural Science, North-West University (Mafikeng Campus), Private Bag X2046, Mmabatho 2735, South Africa
[5] Department of Chemistry, Faculty of Natural and Agricultural Science, North-West University (Mafikeng Campus), Private Bag X2046, Mmabatho 2735, South Africa
* Correspondence: ebrochima@gmail.com

How To Cite: Okpara, E.C.; Ajiboye, T.O.; Wojuola, O.B.; et al. Development of $AgBiS_2$ Nanoparticle Modified Bulk Screen-Printed Electrodes for Lead (II) and Cadmium (II) Detection. *Electrochemical Engineering* **2025**, *1*(1), 2.

Highlights

- Enhanced Electrochemical Performance: The $AgBiS_2$-modified screen-printed electrode (MSPE) exhibited significantly lower charge transfer and improved sensitivity for the Pb^{2+} detection compared to the bare electrode.
- Detection Limits and Sensitivity: The sensor achieved a Pb^{2+} LoD of 4.41 ppb, below the WHO limit (10 ppb), while Cd^{2+} had a LoD of 13.83 ppb, above the WHO limit (5 ppb).
- Real-Time Environmental Monitoring: The sensor is suitable for field applications, enabling rapid and cost-effective detection of Pb^{2+} in drinking water.
- Future Improvements for Broader Applications: While effective for Pb^{2+}, further optimization is required to lower Cd^{2+} detection limits, making the sensor more versatile for comprehensive heavy metal monitoring.

Received: 18 April 2025
Revised: 16 June 2025
Accepted: 24 June 2025
Published: 27 June 2025

Abstract: The development of a screen-printed electrochemical sensor for the simultaneous detection of lead (Pb^{2+}) and cadmium (Cd^{2+}) ions in water is reported. A novel $AgBiS_2$ nanoparticle (NP)-modified nanocarbon black (NCB) paste was fabricated and analysed using electrochemical impedance spectroscopy (EIS) and square-wave voltammetry (SWV). The modification significantly enhanced electrode performance by reducing the charge transfer resistance threefold, resulting in improved sensitivity. Under optimized conditions (90-s deposition at −1.2 V in 3 mM HCl, the sensor exhibited clear, well-defined peaks for Pb^{2+} and Cd^{2+}, with detection limits of 4.41 ppb and 13.83 ppb, over a linear current concentration range of 50–200 ppb, respectively. The Pb^{2+} detection limit was below WHO-recommended levels, demonstrating the electrode's suitability for real-time environmental monitoring. This cost-effective disposable sensor paves the way for potable, high-performance heavy metal sensing applications.

Keywords: electrochemical sensor; $AgBiS_2$ nanoparticles; screen-printed electrode; heavy metal detection; water quality monitoring

1. Introduction

Water and its resources are crucial to supplying nutrients and providing a conducive habitat for all organisms. However, rapid population growth and industrial expansion have significantly increased the demand for freshwater, placing immense pressure on its availability and quality [1]. The indiscriminate use and subsequent discharge of substances such as polyethylene and plastic bags, fertilizers, pesticides, sewage wastes, eutrophication, domestic wastewater, mining wastes, oil spills, radioactive wastes, thermal pollution, and acid rains into water bodies lead to heavy metal accumulation and pollution of the environment [2].

Heavy metals (HMs) are metals with a density above 5000 kg/m^3 [3]. Environmental pollution by heavy metals and metalloids is are global environmental challenge and poses great threats to human health, organisms, and the ecosystem in general [4–6]. Owing to their ubiquitous nature, HMs are the most prevalent of the water resources pollutants and are thus employed as water quality monitoring parameters [7]. These pollutants can generate harmful effects on aquatic fauna and flora and can cause various health problems in organisms and humans by entering the food chain [8]. Hence, constant environmental and water quality assessment of heavy metal pollution is crucial [9].

Various advanced spectroscopic techniques have proven invaluable in quantifying heavy metals across different media, including environmental samples, industrial processes, and biological materials. Notable methods include X-ray fluorescence (XRF), which provides rapid, non-destructive analysis and is particularly effective for identifying elemental composition in solids [10]. Inductively coupled plasma mass spectroscopy (ICP-MS) is renowned for its sensitivity and precision, allowing for the detection of trace levels of metals, even in complex matrices. In contrast, inductively coupled plasma optical emission spectroscopy (ICP-OES) offers simultaneous multi-element analysis with high throughput, making it suitable for bulk quantification of metals. Ultraviolet-visible (UV-vis) spectrometry, while less specific for heavy metals, is commonly employed for determining their concentrations in solution through the use of colorimetric methods [11]. Furthermore, laser-induced breakdown spectroscopy (LIBS) provides a rapid and versatile way to analyze metals in a variety of states, from solid to gaseous, by measuring the light emitted from a plasma created by laser ablation of the sample. Together, these advanced techniques enhance our ability to monitor and manage heavy metal contamination in diverse environments, ensuring better public health and safety [10,11].

However, common challenges such as high equipment costs, the need for sample collection and digestion, the requirement for advanced technical skills, and time-consuming procedures limit their widespread application. Meanwhile, electroanalytical techniques have the advantage of portability, eco-friendliness, reliability, and rapid sensing. They also have the advantage of high sensitivity and selectivity towards HM ions. Various electrochemical sensors and techniques have been successfully and comparably employed in the quantitation of HMs in water [12]. With the use of printing technology, cost-effective, electroactive, and disposable screen-printed electrodes could be mass and simply produced to meet the expanding need for decentralized environmental monitoring of HMs [9,13,14].

The material composition of the working electrode (WE) in the electrochemical sensing platform plays a key role in the performance of the setup. Graphitic carbon, graphite, nano-graphite, nano carbon black, as well as a host of other carbon-based materials, have been extensively reported as electroactive materials for electrochemical applications [15–17]. These materials possess excellent chemical stability, electrical conductivity, broad potential range, structural versatility, rich carbon-carbon bonds (internally and externally), and abundant surface groups [18]. The incorporation of electroactive nanomaterials on the surface of the working electrodes has been reported to show better current response than the unmodified counterparts [19–22].

Adsorption, which involves non-covalent bonding between the modified suspension and the surface, is one of the surface modification approaches. They include self-assembled monolayers, chemical adsorption, and coatings (dip coating [23], spin coating [24], and drop casting [25]). The drop-casting method, widely used for electrode modification, involves applying a solvent-modifier mixture onto the bare working electrode (WE) surface, allowing the solvent to evaporate and leaving a uniform coating on the surface [26]. However, this surface modification possesses some inherent limitations, such as uneven distribution of the modifier on the surface of the WE and poor cycling ability. To overcome these challenges, an alternative strategy involves incorporating the modifying material directly into the electrode ink. This approach has been explored to improve the detection of heavy metals such as Cu^{2+}, Cd^{2+}, Pb^{2+}, and Zn^{2+} [27–29]. Embedding the modifier within the bulk of the electrode ensures a more uniform distribution, thereby enhancing the reproducibility and overall electrochemical performance. For instance, one study reported the development of a bulk-modified screen-printed electrode (SPE) by blending bismuth oxide (Bi_2O_3) with carbon ink, which facilitated effective stripping analysis of Pb^{2+} and Cd^{2+} in soil and water samples via chronopotentiometry [30].

Silver bismuth sulphide is a ternary material that has attracted attention due to its unique characteristics and diverse applications. Silver has frequently been employed in the design of electrochemical sensors due to its low cost and excellent electrical conductivity [31]. Its unique properties, including high electroactivity and a tendency to form stable silver ions [32], make it an ideal material for enhancing the sensitivity and accuracy of various sensor applications. Additionally, silver's ability to facilitate faster electron transfer rates [33], can significantly improve the performance of sensors used in detecting chemical substances and monitoring environmental parameters. This combination of affordability and superior performance continues to drive research and innovation in developing silver-based electrochemical sensors [34,35].

Bismuth-based electrodes, in addition to their low cost, offer advantages such as enhanced peak separation [36,37], a wide linear dynamic range, and a strong signal-to-background ratio. They also exhibit high hydrogen evolution and mitigate the effects of dissolved oxygen in solution [37–39]. While the stripping performance of mercury electrodes results from amalgam formation, bismuth film electrodes function uniquely by forming multicomponent alloys. Bismuth readily forms low-temperature fusible alloys with heavy metals like Pb, Cd, Tl, Sb, In, and Ga, facilitating the nucleation process during metal deposition [37,40].

Therefore, using ternary $AgBiS_2$ nanoparticles in sensing applications offers significant advantages due to the synergistic effects between Ag-Bi metals. This unique combination can enhance the overall efficiency of the sensing mechanism, potentially leading to improved sensitivity and selectivity in detecting target analytes. The distinct electronic properties of Ag and Bi, when integrated into the nanostructure, may facilitate better charge transfer and reduced detection limits, making $AgBiS_2$ a promising candidate for advanced sensing technologies. Additionally, the unique morphological characteristics of these nanoparticles could further optimize their interaction with various environmental factors, thereby broadening their applicability across different sensing platforms [31,41–43].

Thus, a composite of $AgBiS_2$ and carbon-based materials is expected to bring improved electrochemical sensing activities. A study developed a sensor by integrating $AgBiS_2$ with MXene, resulting in a composite that exhibited excellent electrochemical properties. The sensor demonstrated a low detection limit of 0.00254 μM, high sensitivity of 5.862 $\mu A\ \mu M^{-1}\ cm^{-2}$, and a wide linear range from 0.02 to 1869 μM [44]. In a separate study, a novel photoelectrochemical sensor was fabricated using a composite of SnS_2, $AgBiS_2$, and graphene oxide (GO) [45]. These characteristics indicate its potential for sensitive and selective detection of heavy metal ions.

In our previous study, silver bismuth sulphide ($AgBiS_2$) and its composite were synthesized, characterized and utilized as a photocatalyst for remediating heavy metals from water [46]. In the current study, the as-synthesized $AgBiS_2$ was mixed with NCB paste in bulk production of modified SPE for the simultaneous quantitation of Pb^{2+} and Cd^{2+} in water. The $AgBiS_2$/NCB composite modified SPE returned a reduced charge transfer resistance and better current response.

2. Materials and Methods

2.1. Reagents and Materials

All reagents used in this study were of analytical grade. Deionized water with a resistivity of at least 18.2 MΩ·cm, obtained from a Milli-Q Integral 3 system (Millipore UK, Watford, UK), was utilized for all solution preparations. Electroanalytical reagents, including hexaaminеruthenium(III) chloride (98%), hydrochloric acid (37%), and 1000 ppm standard solutions of cadmium and lead, were sourced from Merck (Gillingham, UK) and Sigma-Aldrich (Gillingham, UK). Carbon black (Super P®, >99+%) was procured from Fisher Scientific (Loughborough, UK).

2.2. Synthesis of $AgBiS_2$

$AgBiS_2$ was synthesized using a previously reported method [46]. Briefly, 0.5 mmol (0.243 g) of silver nitrate and 0.5 mmol (0.085 g) of bismuth nitrate pentahydrate were measured into a 100 mL beaker. To this mixture was added 1.0 mmol (0.240 g) of thioacetamide, 1.0 mmol (0.076 g) of sodium sulphide and 50 mL of water. The mixture was stirred for 45 min at 40 °C to obtain a homogenous solution, which was then transferred into 100 mL autoclave and heated for 40 h at 180 °C. At the end of the reaction, the system was left to cool to room temperature and the deep grey solid formed was transferred into a centrifuge tube. The solid formed was separated, washed with absolute ethanol to obtain a pure solid, and dried in a muffle furnace for 8 h at 80 °C.

2.3. Fabrication of Modified Bulk Screen-Printed Electrode

A thin film of carbon ink was deposited manually on the surface of a clean plastic polymer substrate. The plastic plates were dried in the oven at 60 °C, and the dried plates were divided into two: the bare printed electrode plate and the modified electrode. In the modification process of the electrode, about 93 mg of $AgBiS_2$ NPs was mixed evenly with about 1000 mg fresh load of the carbon paste and deposited thinly on a 4 mm end of the second half. The modified bar was subsequently dried under the same condition. A working electrode area of 4 × 4 mm^2 was cut from the bare and modified plate as shown in Figure 1a and used in electroanalysis. Figure 1a,b) illustrate the fabrication process of the screen-printed carbon electrode.

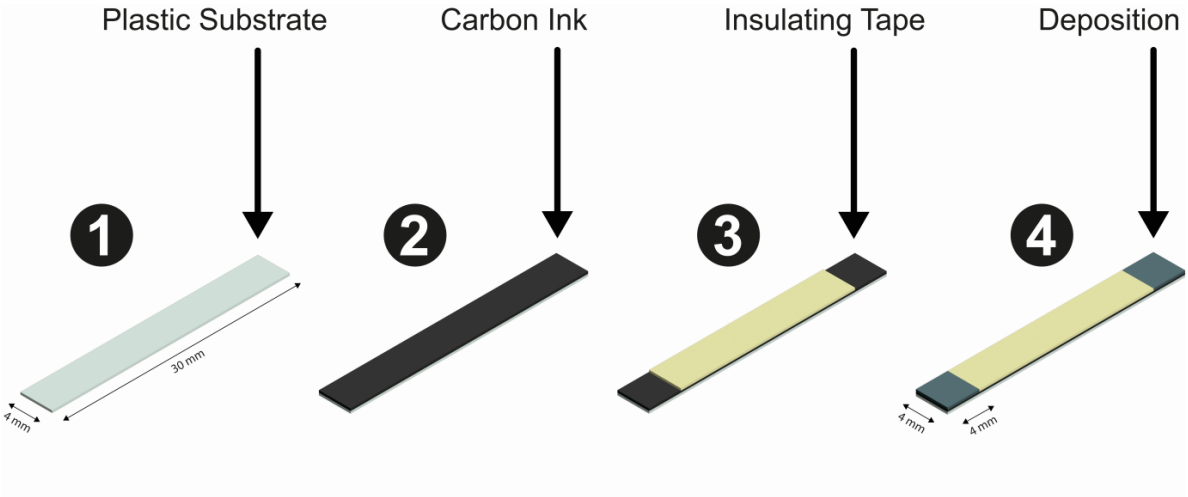

(**a**)

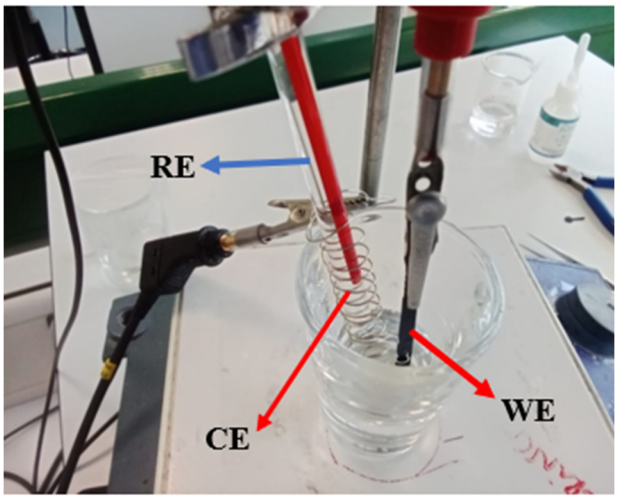

(**b**)

Figure 1. (**a**) Schematic representation of the design of modified screen-printed electrodes (MSPE), (**b**) a typical workstation for MSPE. (WE: working electrode; RE: reference electrode and CE: counter electrode).

2.4. Electrochemical Measurement

2.4.1. Instrumentation

Square wave voltammetry (SWV) measurements were conducted using AutoLab and analysed with NOVA 2.1.6 software. A large 100 mL cell was employed for the electrochemical analysis. The voltammetric measurements involved the vertical placement of a one-electrode screen-printed sensor, connected to an external nichrome wire counter and Ag/AgCl reference electrodes, into the electrolyte solution. To enhance mixing and facilitate standard addition, a convenient stirring process was implemented. Microscopic images of the as-prepared $AgBiS_2$ NPs bulk-modified screen-printed electrode (MSPE) and the bare screen-printed electrode (BSPE) were captured using scanning electron microscopy (SEM) provided by ThermoFisher Scientific, Waltham, MA, USA.

2.4.2. Impedance Measurements

The electrochemical performance of both the bare electrode and the modified electrode was systematically assessed using electrochemical impedance spectroscopy (EIS). This evaluation was conducted in a probe solution containing 5 mM of Ru $(NH_3)_6$. By employing this specific probe, we aimed to gain insights into the charge transfer resistance and overall conductivity of the electrodes. The EIS measurements provided valuable data that allowed us to interpret the effects of the modification on the electrode's electrochemical behaviour, offering a detailed comparison of their performance characteristics.

2.4.3. Electrical Characterization of the Electrode

A common observation of using screen-printed electrodes is the distinctions in current response between different mass-produced SPEs. A multimeter was used to measure the electrical current resistance between two equal distances for about 12 pieces of 30 × 4 mm^2 electrode bars. To further validate the possible improvement in the conductivity of the modified electrode plate, the resistance between two diagonal distances in 600 × 300 mm^2 of the bare/unmodified and modified printed screens was measured.

2.4.4. Electrochemical Quantitation of the Analytes

The SPE was positioned in a cell, and the conditioning of the electrode surfaces was performed to achieve a stable response and establish an appropriate baseline. This process involved applying five CV cycles ranging from −0.2 V to −0.7 V, a step potential of 10 mV, a conditioning time of 15 s, and a conditioning potential of +0.2 V. The scan rate was set at 0.05 Vs^{-1} in a solution of 100 mmol L^{-1} HCl. Following this, 50 mL of deionized water was introduced into the cell, and square wave voltammetry (SWV) measurements were conducted.

The optimized SWV technique utilized the following parameters: a deposition potential of −1.2 V for 90 s (with stirring at 1000 rpm), a conditioning (cleaning) potential of +0.1 V for 15 s, potential range of −0.9 to −0.35 V, an equilibration time of 10 s, a step potential of 6 mV, an amplitude of 40 mV, and a frequency of 25 Hz. The potential windows were adjusted according to the peak potential values of cadmium and lead ions. All applied potentials throughout the study were referenced against the Ag/AgCl electrode, and no de-aeration was necessary.

Bulk stripping voltammetric responses were used for peak current measurements without blank subtraction. Simultaneous quantitation of the analytes was conducted using the standard addition method. Limits of detection (LoD) and quantification (LoQ) were calculated as 3 × SD/m and 10 × SD/m, respectively, where SD represents the standard deviation of the three scans of the lowest analyte concentration, and m is the slope of the calibration curve. For optimal stripping performance, a broader potential window than used here is recommended.

3. Results and Discussion

3.1. Impedance and Surface Characterization of the SPE

To provide a more comprehensive analysis of the impedance characteristics of the Screen-Printed Electrode (SPE), we opted for an adapted Randles equivalent circuit model to interpret the measured data more effectively. In this context, the Randles equivalent circuit was utilized to fit the impedance data depicted in Figure 2, incorporating key circuit parameters: solution resistance (Rs), charge transfer resistance (Rp), and the Constant Phase Element (CPE). The solution resistance (Rs) accounts for the intrinsic resistance of the electrolyte between the electrode interfaces, while the charge transfer resistance (Rp) is indicative of the kinetics of the electrochemical reaction occurring at the electrode surface. Additionally, the CPE is employed to provide a more accurate representation of the non-ideal capacitive behaviour observed in the system, reflecting surface inhomogeneities or roughness [47–49].

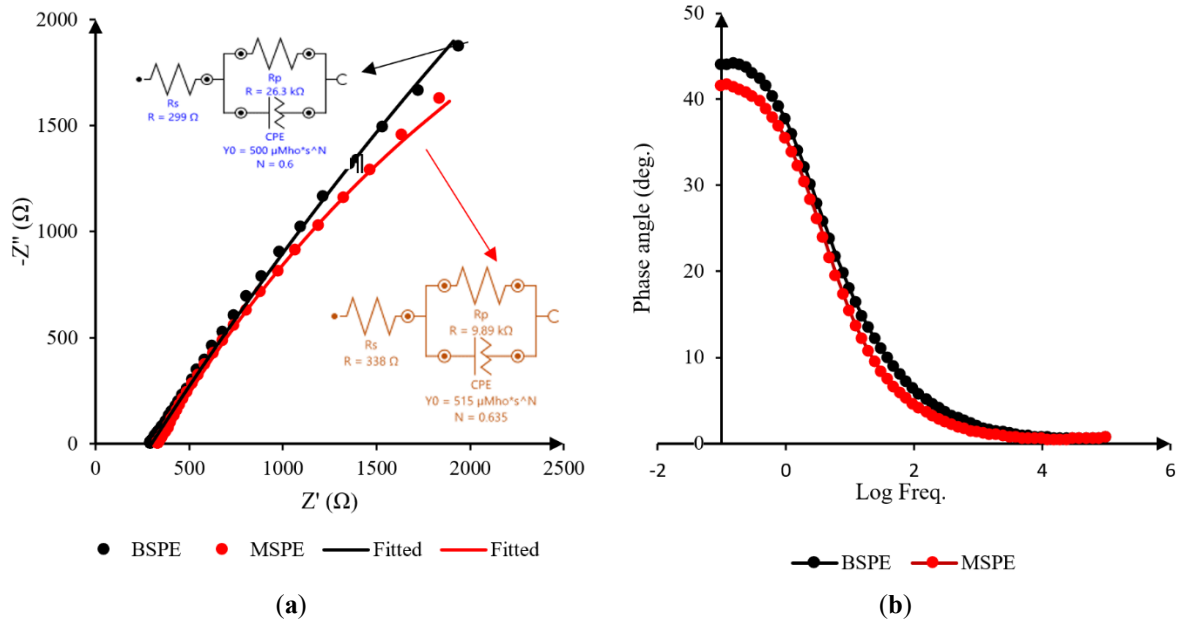

Figure 2. The (**a**) Nyquist (inset: Randle equivalent circuit), and (**b**) Bode plot for BSPE and MSPE. Frequency range (0.1 MHz to 0.1 Hz; amplitude of 0.01 V in 1 mM of hexaaminеruthenium(III) chloride $[Ru(NH_3)_6]^{3+}$ in 0.1 M KCl.

From the equivalent circuit analysis, the MSPE exhibits a slightly higher solution resistance (Rs = 338.14 Ω) compared to the BSPE (Rs = 299.09 Ω). The slightly higher Rs observed for the MSPE compared to the BSPE suggests that the modification introduces a minor additional resistance in the ionic path through the electrolyte, likely due to morphological or structural changes introduced during electrode modification [50,51]. In contrast, the charge transfer resistance (Rp) shows a pronounced difference between the two electrodes. The BSPE displays a much larger Nyquist semicircle, corresponding to an Rp of 26,335 Ω, while the MSPE shows a significantly lower Rp of 9891 Ω. This substantial decrease in Rp reflects enhanced interfacial charge transfer kinetics at the modified electrode surface. The incorporation of $AgBiS_2$ and NCB improves the electrode's electrochemical activity by increasing the active surface area and facilitating electron transport. $AgBiS_2$ provides abundant binding and catalytic sites, while NCB enhances electrical conductivity and promotes effective interaction between the electrode and redox species. It is important to note that in this context, the charge transfer resistance (Rp) reflects the ease with which electrons move across the electrode–electrolyte interface and is a direct indicator of the electrode's electrochemical performance. The marked reduction in Rp for the MSPE confirms the effectiveness of the modification in accelerating charge transfer processes. This drop in Rp agrees with the slight drop in the phase angle from 44° for the BSPE to 41.6° for MSPE (Figure 2a). Previous studies have shown that reduced phase angle is correlated with increased conductivity and hence improved electrochemical performance [52,53]. The electrical current resistance (R Ω) measured for the BSPE and MSPE is 358.7 Ω and 121.8 Ω respectively, agreeing with the EIS study. A lower Rp value is desirable in sensing applications as it enables faster and more efficient electron transfer.

Figure 3a–d presents SEM images of the BSPE and the MSPE. While the overall external morphology appears similar between both electrodes, distinct surface features are visible in the MSPE images (Figure 3a,c), particularly in the regions highlighted in red. These features are absent in the BSPE images (Figure 3b,d) and are attributed to the presence of MSPE nanocomposite domains deposited via ink-mixing. Such agglomerated or unevenly distributed regions are typical of this modification approach and are consistent with literature reports of nanocomposite incorporation onto carbonaceous electrode surfaces [54], confirming successful surface functionalization. The MSPE exhibits a slightly higher degree of electrochemical homogeneity, as indicated by its N value of 0.63 compared to 0.60 for the BSPE (Table 1). Both electrodes exhibit low χ^2 values (BSPE: 0.00, n = 28; MSPE: 0.004, n = 32), confirming a good fit of the impedance model. The lower χ^2 for MSPE indicates that the modified electrode has a slightly better data-model correlation.

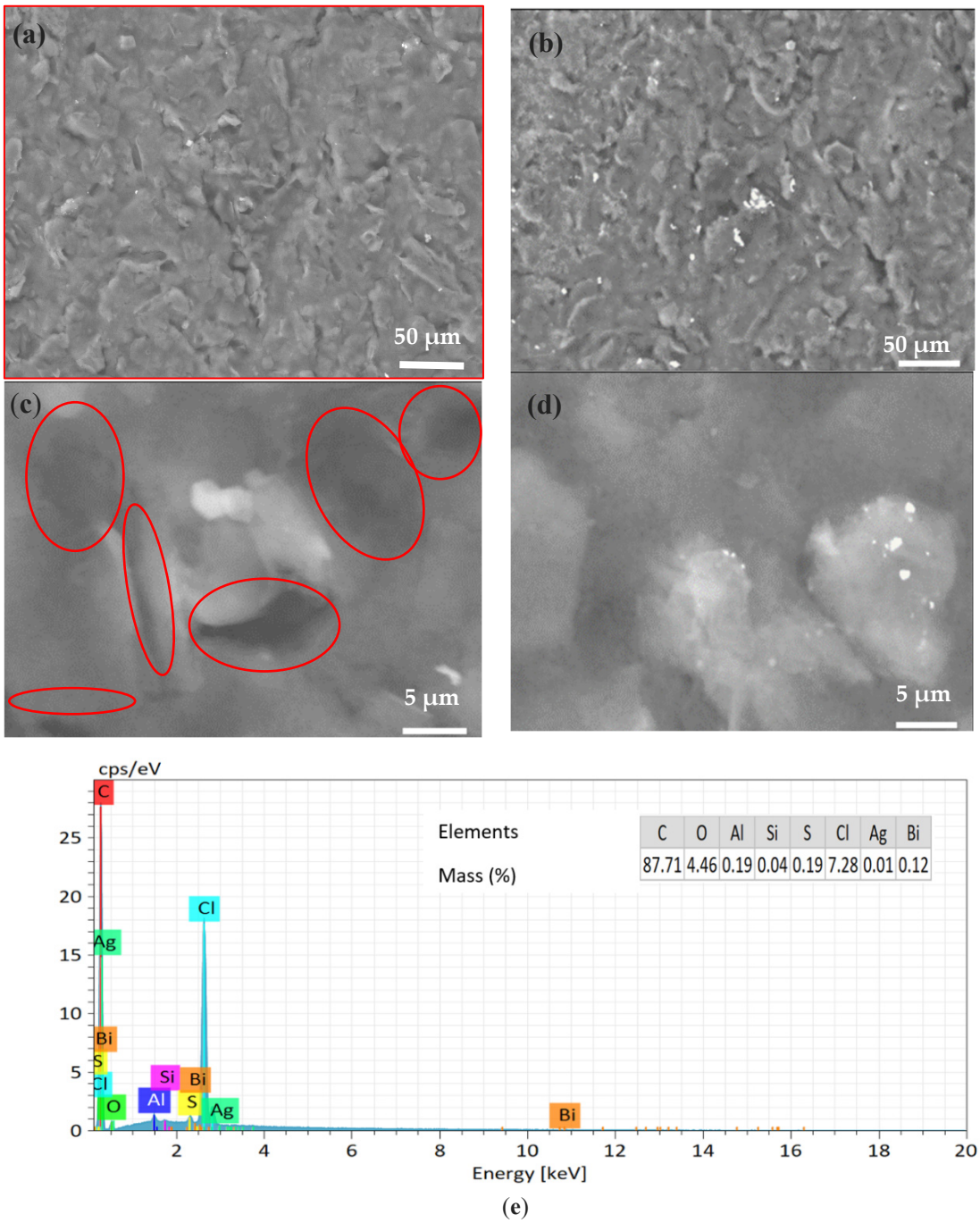

Figure 3. SEM images of (**a**,**c**) MSPE and (**b**,**d**) BSPE at different magnifications. The red-circled regions in images (**a**,**c**) highlight morphological features, such as agglomerated particles and increased surface roughness, indicative of successful surface modification. These features are absent in the bare SPE images (**b**,**d**), confirming the presence of the modifying layer and (**e**) the EDX of used MSPE.

Table 1. The EIS fit data for the BSPE and MSPE in probe solution. Figures in parenthesis are error values.

Electrode	Rs (Ω)	Rp (Ω)	N	χ^2	Phase Angle (deg.)
BSPE	299.09 (0.22)	26335 (13.04)	0.6	0.007	44
MSPE	338.14 (0.16)	9891 (4.14)	0.64	0.004	41.6

The energy-dispersive X-ray spectroscopy (EDX) spectrum (Figure 3e) provides insights into the elemental composition of the electrode surface. Carbon is the most dominant element at 87.71%, primarily due to the use of nanocarbon black as a conductive material. Oxygen is detected at 4.46%, likely from surface oxidation or electrolyte interactions, while chlorine is present at 7.28%, possibly related to hydrochloric acid used in the experiments. Silver, at 0.01%, and bismuth, at 0.12%, are associated with the $AgBiS_2$ material, which plays a key role in detecting heavy metals. Sulfur is detected at 0.19%, confirming its presence in the compound. Trace

elements like silicon (0.04%) and aluminum (0.19%) may arise from impurities or environmental contamination. Overall, the analysis underscores the substantial carbon content, validates the integration of $AgBiS_2$, and indicates potential surface interactions with the electrolyte.

The elemental analysis using EDX revealed relatively low surface concentrations of Ag (0.01%) and Bi (0.12%) on the modified electrode. While this might suggest minimal modifier presence, it is important to note that EDX provides semi-quantitative [55], surface-localized data, typically limited to a penetration depth of 1–2 microns. As such, the results may not fully reflect the total content of $AgBiS_2$ embedded within the carbon matrix particularly in ink-mixed or porous systems where materials may be distributed throughout the electrode volume [56–58]. Despite the low EDX values, the modified electrode demonstrated significantly enhanced electrochemical responses, including increased peak currents and reduced charge transfer resistance, indicating that the modifier is electrochemically active and functionally present in sufficient amounts. However, it is possible that non-uniform dispersion or partial agglomeration of MSPE may contribute to localized variations in active site availability, which could affect the reproducibility and sensitivity of the sensor, particularly at lower analyte concentrations. To address this uncertainty and strengthen future studies, a bulk quantification method such as inductively coupled plasma–optical emission spectrometry (ICP-OES) or mass spectrometry (ICP-MS) will be considered to accurately determine the total loading of Ag and Bi in the electrode formulation. This approach would provide more representative data on modifier concentration and distribution, enabling a more precise correlation between material loading and electrochemical performance.

3.2. Voltammetric Detection method

Although $AgBiS_2$ NP is attracting more research attention due to its unique properties in various environmental applications [59], its potential in reliable and simple real-time electroanalysis is yet to be fully explored. This study aims to validate the amplifying current response of NCB paste modified with $AgBiS_2$ in the simultaneous quantitation of Cd^{2+} and Pb^{2+} in a water medium. Such validation would be followed with bulk production of a three-screen-printed electrode system based on carbon ink/$AgBiS_2$ mixture WE for application in real-time environmental water quality monitoring. In this study, the SWV technique is proposed because of the robust analytical sensitivity of stripping techniques, thus making them suitable for the simultaneous quantitation of trace HMIs in eco-water [26].

In square wave voltammetry (SWV), the detection of Pb^{2+} and Cd^{2+} using an $AgBiS_2$ NP/NCB-modified electrode operates via electrochemical accumulation and stripping. $AgBiS_2$ plays a dual functional role: (i) *Chemical Affinity*: Sulfide (S^{2-}) ions in $AgBiS_2$ form strong coordination bonds with heavy metal ions such as Pb^{2+} and Cd^{2+}, while Bi^{3+} can also chelate these ions through surface interactions [60–64]. This enhances the preconcentration of target ions on the electrode surface. (ii) *Electrocatalytic Activity***:** $AgBiS_2$ improves electron transfer kinetics at the electrode–electrolyte interface, reducing the overpotential required for the redox processes, and increasing signal intensity [31,65]. During the accumulation step, metal ions are adsorbed onto the modified electrode via electrostatic attraction and chemical complexation. Upon applying a negative potential, Pb^{2+} and Cd^{2+} are electrochemically reduced to Pb^0 and Cd^0, depositing on the electrode surface. In the stripping phase, the deposited metals are reoxidized to Pb^{2+} and Cd^{2+} under a positive potential, generating characteristic peak currents proportional to their concentrations [66]. The presence of NCB increases the electrode's effective surface area, further enhancing ion adsorption and charge transfer.

Mechanism of electrochemical reactions involved

Step 1: Preconcentration

For lead: $Pb^{2+}_{(aq)} + 2e^- \rightarrow Pb^0_{(s)}$

For cadmium: $Cd^{2+}_{(aq)} + 2e^- \rightarrow Cd^0_{(s)}$

Step 2: Stripping/reoxidation

For lead: $Pb^0_{(s)} \rightarrow Pb^{2+}_{(aq)} + 2e^-$

For cadmium $Cd^0_{(s)} \rightarrow Cd^{2+}_{(aq)} + 2e^-$

Figure 4a shows the SWV scans between the potential windows of −0.9 to −0.35 V. The blue line shows minimal current response across the potential range. This represents the electrode response in the absence of the target analyte, indicating low background noise or minimal interference. A small peak emerges at approximately −0.8 V (corresponding with oxidation of Cd^{2+}) and another at −0.5 V (corresponding to the oxidation of Pb^{2+} in

50 ppb analyte (red line) solution. The peak current is significantly higher than the blank, showing the electrode's capability to detect low analyte concentrations. The peak current is substantially higher in 250 ppb analyte (black line) compared to 50 ppb, reflecting a clear concentration-dependent response.

These well-defined peaks suggest high sensitivity and selectivity of the electrode. The modified electrode thus demonstrated the capacity for successful simultaneous electrochemical stripping of Cd^{2+} and Pb^{2+} ions, with clear distinct peaks. However, at higher concentrations, the peak widens, and the potential gaps close. The values of the oxidation peak current (i_{pa}) for the Cd^{2+} and Pb^{2+} ions were 19.82 µA at a potential voltage of ~−0.5 V and 11.80 µA at ~−0.8 V respectively in the presence of 250 ppb of the analyte indicating that the modified electrode has a preference towards the stripping of the Pb^{2+} than the Cd^{2+}. This preference could be attributed to factors such as favourable redox potential, higher surface affinity, and more efficient electron transfer kinetics for Pb^{2+} ions [67,68].

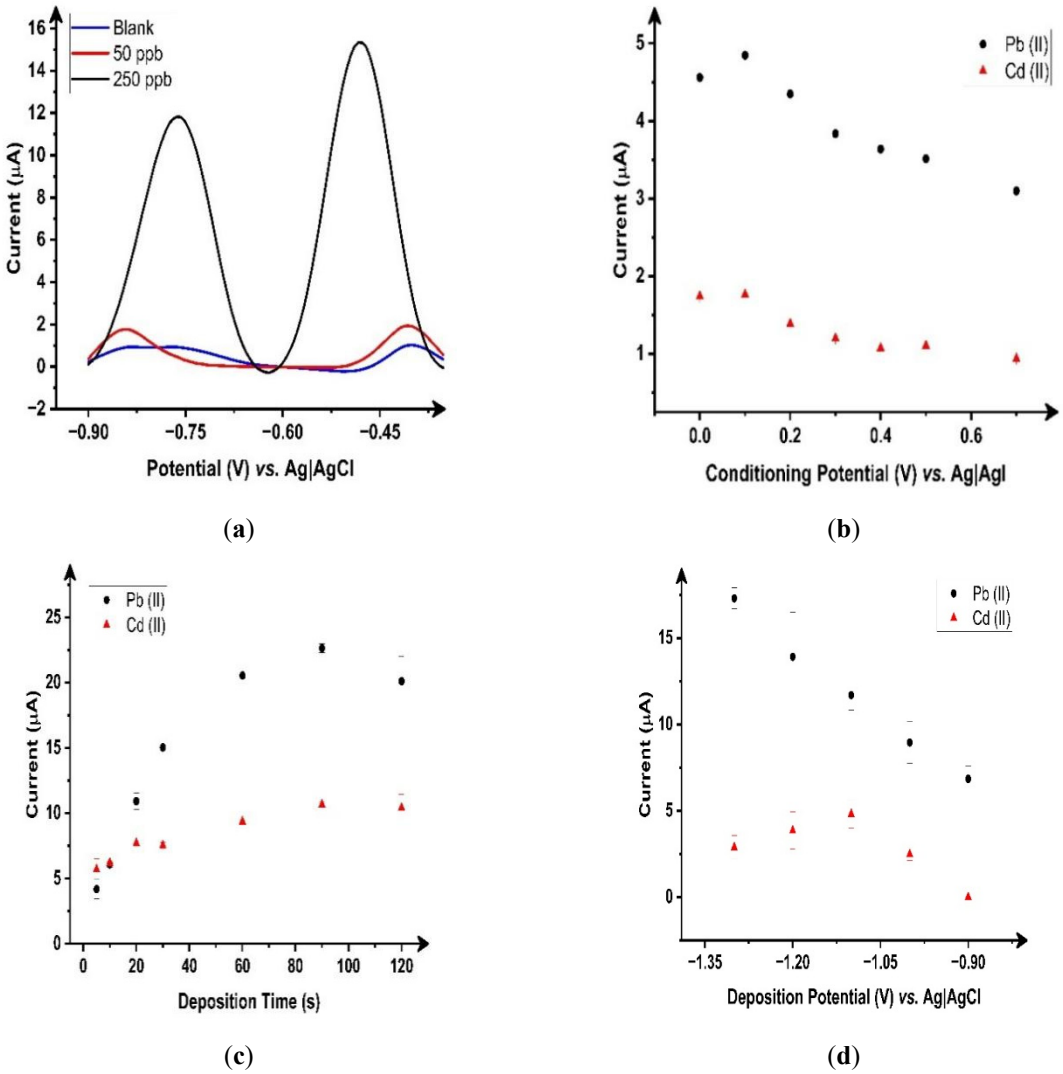

Figure 4. (**a**) Square wave voltammetry (SWV) response at the MSPE in 3 mM HCl electrolyte, recorded under different conditions: absence of analyte (blue), presence of 50 ppb analyte (red line), and 250 ppb analyte (red). Variation in peak current magnitude for Cd^{2+} and Pb^{2+} as a function of (**b**) conditioning potential, (**c**) deposition time and (**d**) deposition potential measured in the presence of 100 ppb analytes. Experimental parameters: 90 s deposition time, deposition potential of −1.2 V, equilibration time of 10 s, conditioning potential of 0.1 V for 15 s, step potential of 6 mV, modulation amplitude of 40 mV, and a frequency of 25 Hz. Electrodes used: nichrome wire as the counter electrode and a silver reference electrode (N = 3 consecutive runs performed on a single electrode).

Keeping other stripping parameters such as amplitude, frequency, and step potential at 40 mV, 25 Hz, and 6 mV respectively, within the range of the analogous values previously reported for the stripping of Pb^{2+} [69,70], the pH of the electrolyte, deposition potential, conditioning potential, and deposition time were varied in this study to determine how these parameters affect the stripping performance of the electrode.

To clean the surface of the electrode, minimize variations in the voltammograms, and improve the stability of electrochemical signals by minimizing the variations in the surface of the electrode, the surface of the electrode was conditioned before each scan. Therefore, selecting an optimal conditional potential is very pivotal. Fixing other parameters constant, the SWV was scanned between different potentials to determine the optimal conditioning potential (Figure 4b). The i_{pa} increased from 0 V to 0.1 V for Pb^{2+} but remained relatively the same for the Cd^{2+} ion and continued to drop steadily with increasing value of the conditioning potential. Subsequently, each MSPE was conditioned at 0.1 V. Typically, the MSPE was placed into a 50 mL cell and then, five (5) CV cycles were applied at a step potential of 4 mV, a conditioning potential of 0.1 V for 15 s, and a scan rate of 50 mV/s in 0.1 M HCl [71].

The i_{pa} continued to increase with increasing deposition time until 90 s and then declined for Cd^{2+} and Pb^{2+}, which could be attributed to the supersaturation of the surface of the MSPE as shown in Figure 4c. Furthermore, the error bar continued to increase with increasing deposition time. Subsequent electroanalysis was done using 90 s deposition time.

The effect of the deposition potential was evaluated between −1.3 V and −0.9 V using 100 ppb of the analyte solution in 0.003 M of HCl, which is represented in Figure 4d. The intensity of the i_{pa} continued to increase with increasing negative potential for Pb^{2+} and declined for Cd^{2+} after −1.2 V. Since the current response of Cd^{2+} was already lower than that of the Pb^{2+} and a simultaneous detection system was being considered, the deposition potential of −1.2 V was chosen and applied in the remaining part of the study.

During the experiments, a constant stirring of 1000 rpm was maintained for the pre-treatment. Considering conditions that could be easily related to real-time field analysis, the lab-based stripping analysis was carried out in quiescent solutions, with an equilibration time of 15 s.

The choice of the electrolyte and the pH of the solution also play another key role in the electrochemical response of an electrode. In this work, the optimal pH was determined by the concentration of the HCl with the highest current response, which would support the simultaneous detection of Cd^{2+} and Pb^{2+} with distinct and clear peaks. HCl was chosen because of its common application in the quantitation of heavy metals in water [9]. As a result, the influence of the chlorine concentration on the magnitude of the peak stripping current was carefully investigated. Figure 5 shows that at 0.0001 M HCl concentration (blue line), there is a very weak current response, while the magnitude of i_{pa} is clear, highest and distinct in 0.003 M HCl concentration (red line). As the concentration of HCl begins to increase, the sensitivity of the electrode begins to wane due to the degradation of the electrode surface [71]. At 0.1 M concentration, the peak potential of Pb^{2+} shifted to the right (higher energy input required), with no current response for the Cd^{2+} ion. Consequently, the 0.003 M HCl was selected as the optimum concentration and employed throughout the study, while closing the potential windows to reduce signal noise to the left.

The concentration of HCl plays a significant role in this detection mechanism, influencing both peak shifts and current responses. This influence is attributable to changes in ionic strength, which affects metal ion adsorption, and complexation effects, such as the formation of $PbCl_4^{2-}$ or $CdCl_4^{2-}$, which can modify the oxidation and reduction behaviors [13]. The surface charge of the electrode is also impacted, thus altering the interactions between the metal ions and the $AgBiS_2$ [72]. From a previous report by Bernalte et al. [70], the current response as a function of HCl concentration was evaluated on four different concentrations (0.001, 0.01, 0.1 M) and the optimal concentration was at 0.001 M. However, the difference between 0.001 and 0.01 is broad, and the optimal HCl concentration should lie somewhere between these values. On evaluation, the optimal value was at 0.003 M. Relative to a broader four HCl concentrations (0.0001, 0.003, 0.01, 0.1 M) as shown in Figure 5, the magnitude of i_{pa} at 0.003 M was confirmed as the highest, while 0.1 M returned the lowest response. Using the 0.003 M HCl, and the optimal conditions, the current signal due to the variations in analyte concentration between 50–3200 ppb was investigated.

A linear relationship was observed for both Cd^{2+} and Pb^{2+} in the concentration ranges of 50–200 ppb and 200–3200 ppb, demonstrating the MSPE's capacity to function effectively across both low and high concentration regimes (Figure 6). The LoDs in the lower concentration range, calculated using the 3σ method, were 4.41 ppb (R^2 = 0.992) for Pb^{2+} and 13.83 ppb (R^2 = 0.979) for Cd^{2+}. According to World Health Organization (WHO) guidelines, the maximum permissible limits for Pb^{2+} and Cd^{2+} in drinking water are 10 ppb and 5 ppb, respectively. These results indicate that the MSPE method achieves a LoD below the regulatory threshold for Pb^{2+}, making it a viable tool for monitoring trace levels of lead in water. However, the current LoD for Cd^{2+} remains above the WHO threshold, which presents a limitation for applications involving ultra-trace detection in drinking water. This elevated LoD may be attributed to factors such as partial agglomeration of MSPE on the electrode surface [73], competitive ion interference [74,75], and variability in surface adsorption dynamics for Cd^{2+} [76]. To address this, future optimization strategies could include refining the nanocomposite distribution through surfactant-assisted

ink mixing [77,78], increasing the density of electroactive binding sites, or integrating in situ bismuth film deposition to enhance Cd^{2+} affinity [79]. Despite this limitation, the sensor remains suitable for environmental samples where Cd^{2+} concentrations typically exceed WHO limits, and ongoing refinement may further improve its trace-level detection capabilities.

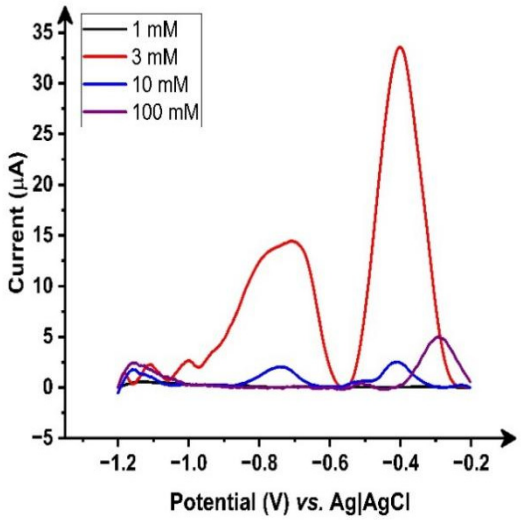

(**a**)

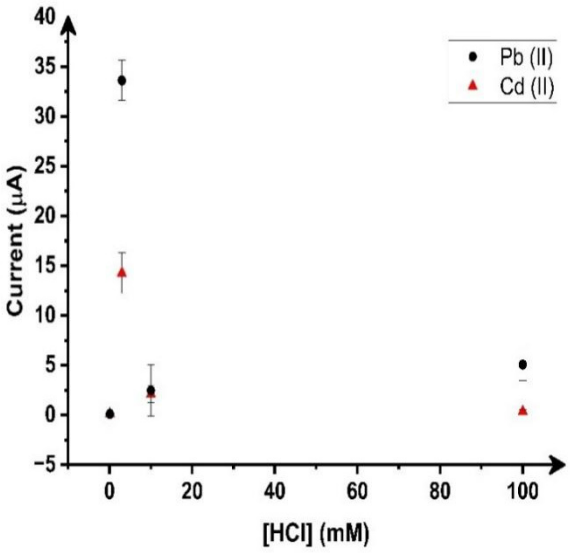

(**b**)

Figure 5. The relationship between the peak current magnitude of Cd^{2+} and Pb^{2+} and pH (corresponding to HCl concentration) in (**a**) SWV mode, (**b**) oxidation current vs HCl concentration, in the presence of 100 ppb of the analyte solution. The experimental conditions include a deposition time of 90 s, a conditioning potential of 0 V for 5 s, a step potential of 5 mV, a modulation amplitude of 20 mV, and a frequency of 25 Hz. The electrode setup consists of a nichrome wire as the counter electrode and a silver electrode as the reference (N = 3 consecutive runs performed on a single electrode).

At higher concentrations and over a broader detection range, the LoDs for Cd^{2+} and Pb^{2+} were determined to be 168 ppb (R^2 = 0.995) and 39.47 ppb (R^2 = 0.996), respectively. These values exceed the permissible limits for both drinking water and seawater, suggesting that the method is also suited for applications involving higher analyte concentrations as well as trace-level detection in compliance with drinking water standards. The presence of two different linear ranges in the calibration plots (Figure 6b,c) suggests that the electrochemical response follows a dual-regime behavior based on concentration. At lower concentrations, the sensor follows a linear response due to direct adsorption of Pb^{2+} and Cd^{2+} onto the electrode surface, ensuring an efficient electron transfer. At higher concentrations, the sensor surface starts to reach saturation, leading to a deviation in response. In this

regime, the adsorption sites become limited, and additional metal ions may be interacting differently (e.g., forming multilayers or undergoing diffusion-controlled processes) [80–82]

The performance of the MSPE is also comparable to other carbon-based electrodes reported in the literature, as represented in Table 2.

Table 2. Detection of Pb^{2+} and Cd^{2+} in water samples with MSPE: performance comparison with carbon-based SPEs.

Electrode	Detection Limit (ppb)		Linear Range (ppb)		DT (s)	Technique	Ref.
	Pb^{2+}	Cd^{2+}	Pb^{2+}	Cd^{2+}			
CPE/AC	51.40	44.41	79.5–878	95–427	300	SWV	[83]
SPIL-GrE	93	150	250–2500		–	SWV	[13]
ZnNPs@CF/GLN	8.28	11	16.56–3312	18.33–1833	–	DPV	[84]
BiOCl/CPE	0.42	0.76	10–400	10–450	300	SWV	[85]
GCE-GO-BiNPs	6.22	2.92	20.72–292.15	11.24–158.48	120	SWV	[86]
CPE/CM	78.81	96.17	250–12500	250–12500	70	SWV	[87]
MSPE	4.41	13.83	50–200	50–200	90	SWV	This work
	39.47	168	150–3200	200–3200	90	SWV	This work

CPE/AC: Carbon paste electrode/activated carbon; SPIL-GrE: screen-printed ionic liquid-graphene electrode; CPE/CM: chemically modified carbon paste electrode; DT: deposition time.

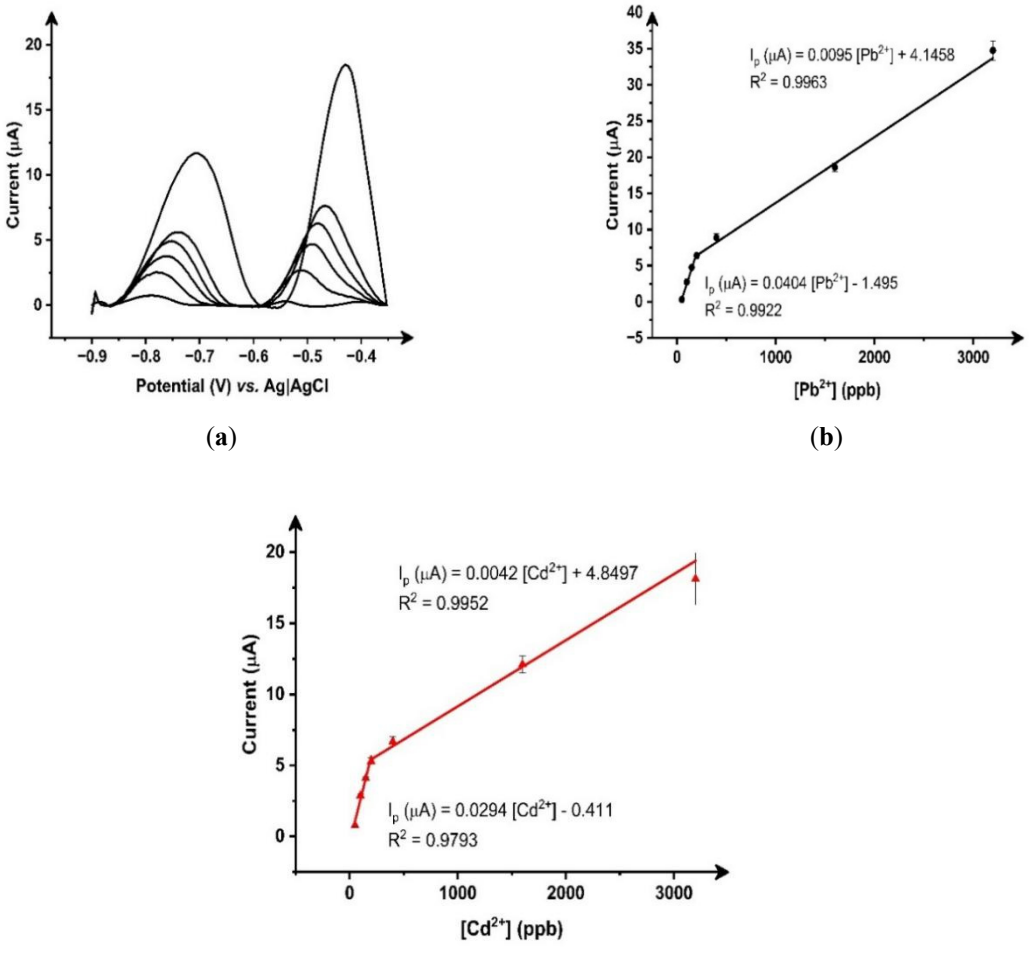

Figure 6. (**a**) The peak current magnitude of Cd^{2+} and Pb^{2+} as a function of concentration (50–1600 ppb), (**b**) Calibration curve for concentrations ranging from 50 to 200 ppb, and (**c**) Calibration curve for concentrations from 200 to 3200 ppb. Experimental conditions include a deposition time of 90 s, an equilibration time of 10 s, a conditioning potential of 0.1 V applied for 15 s, a step potential of 6 mV, a modulation amplitude of 40 mV, and a frequency of 25 Hz. The electrode configuration consists of a nichrome wire as the counter electrode and a silver electrode as the reference (N = 3 consecutive runs performed on a single electrode).

While this study focused on establishing the core detection performance of the MSPE, a full interference study, particularly involving coexisting ions such as Zn^{2+}, Cu^{2+}, and Fe^{2+}, was not conducted. We acknowledge that for practical, real-world applications, understanding the sensor's selectivity in the presence of competing metal ions is critical. Previous studies have shown that bismuth-based systems, such as Bi–Sb alloy-modified carbon paste electrodes, enable simultaneous detection of Zn^{2+}, Cd^{2+}, and Pb^{2+} with minimal signal interference [88], demonstrating that well-engineered modifier systems can achieve robust selectivity even in multicomponent matrices. Inspired by such findings, future work will include a systematic evaluation of the MSPE selectivity, robustness under competitive ion conditions, and real-sample analysis to validate its applicability in complex environmental samples.

4. Conclusions

In this study, a disposable screen-printed electrode (SPE) modified with $AgBiS_2$ nanoparticles (NPs) and nanocarbon black (NCB) was successfully developed for the simultaneous detection of Pb^{2+} and Cd^{2+} in water. The incorporation of $AgBiS_2$ NPs significantly enhanced the electrode's conductivity, charge transfer, and overall electrochemical performance. Electrochemical impedance spectroscopy (EIS) confirmed a threefold reduction in charge transfer resistance (Rp) in the modified SPE (MSPE) compared to the bare SPE (BSPE), demonstrating improved electron transfer kinetics. Scanning electron microscopy-energy-dispersive X-ray spectroscopy spectrum (SEM-EDX) further revealed a more conductive electrode surface, contributing to enhanced analytical performance. Square wave voltammetry (SWV) results showed well-defined oxidation peaks for Pb^{2+} and Cd^{2+} with a clear concentration-dependent response. The computed limits of detection (LoD) were 4.41 ppb ($R^2 = 0.992$) for Pb^{2+} and 13.83 ppb ($R^2 = 0.979$) for Cd^{2+}. Notably, while the LoD for Pb^{2+} falls below the WHO permissible limit, making the electrode suitable for practical environmental monitoring, the LoD for Cd^{2+} remains above regulatory thresholds, highlighting a key performance limitation. In addition, real-sample validation and field deployment studies were not conducted, and sensor stability, both short- and long-term, has yet to be systematically assessed. These gaps underscore the need for further optimization and testing.

Future work will focus on improving Cd^{2+} detection by refining the nanocomposite dispersion and increasing modifier loading, conducting interference studies involving common competing ions such as Zn^{2+}, Cu^{2+}, and Fe^{2+}, and validating the sensor's performance in real water samples, including surface water and industrial effluents. Long-term repeatability, storage stability, and robustness under field conditions will also be evaluated. Additionally, efforts will be directed toward scaling up fabrication using automated screen-printing technology for low-cost, mass production. Collectively, these advancements will help transform this MSPE into a reliable, accessible, and scalable electrochemical platform for real-time heavy metal detection, with significant implications for water quality monitoring, environmental safety, and public health protection.

Author Contributions

E.C.O.: methodology, investigation, writing—original draft preparation, writing—reviewing and editing; T.O.A.: methodology, investigation, writing—reviewing and editing; O.B.W.: validation, writing—reviewing and editing; supervision, funding; D.C.O.: investigation, writing—original draft preparation, writing—reviewing and editing; supervision, validation, funding; E.B.: conceptualization, methodology, investigation; R.D.C.: conceptualization, methodology, investigation, visualization, writing—reviewing and editing; M.J.W.: visualization, software; C.E.B.: conceptualization, methodology, investigation, writing—original draft preparation, writing—reviewing and editing, supervision, validation, software, funding.

Funding

This project was funded by the National Research Foundation [NRF, Reference–SRUG210430598428] grant number [138066], South Africa, in collaboration with the Faculty of Science and Engineering, Manchester Metropolitan University, Manchester, United Kingdom.

Institutional Review Board Statement

Not applicable.

Informed Consent Statement

Not applicable.

Data Availability Statement

The data supporting the findings of this study are available from the corresponding author upon reasonable request.

Conflicts of Interest

The authors declare no conflict of interest.

References

1. Altunkaynak, F.; Çavuşoğlu, K.; Yalçin, E. Detection of heavy metal contamination in Batlama Stream (Turkiye) and the potential toxicity profile. *Sci. Rep.* **2023**, *13*, 11727. https://doi.org/10.1038/s41598-023-39050-4.
2. Kilic, Z. Water pollution: Causes, negative effects and prevention methods. *İstanbul Sabahattin Zaim Üniversitesi Fen Bilim. Enstitüsü Derg.* **2021**, *3*, 129–132.
3. Ali, H.; Khan, E. What are heavy metals? Long-standing controversy over the scientific use of the term 'heavy metals'–proposal of a comprehensive definition. *Toxicol. Environ. Chem.* **2018**, *100*, 6–19.
4. Antoniadis, V.; Shaheen, S.M.; Levizou, E.; et al. A critical prospective analysis of the potential toxicity of trace element regulation limits in soils worldwide: Are they protective concerning health risk assessment?-A review. *Environ. Int.* **2019**, *127*, 819–847.
5. Mukherjee, I.; Singh, U.K.; Patra, P.K. Exploring a multi-exposure-pathway approach to assess human health risk associated with groundwater fluoride exposure in the semi-arid region of east India. *Chemosphere* **2019**, *233*, 164–173.
6. Wallis, I.; Prommer, H.; Berg, M.; et al. The river–groundwater interface as a hotspot for arsenic release. *Nat. Geosci.* **2020**, *13*, 288–295.
7. Obinna, I.B.; Ebere, E.C. A review: Water pollution by heavy metal and organic pollutants: Brief review of sources, effects and progress on remediation with aquatic plants. *Anal. Methods Environ. Chem. J.* **2019**, *2*, 5–38.
8. Hembrom, S.; Singh, B.; Gupta, S.K.; et al. A comprehensive evaluation of heavy metal contamination in foodstuff and associated human health risk: A global perspective. *Contemp. Environ. Issues Chall. Era Clim. Change* **2020**, *2020*, 33–63.
9. Okpara, E.C.; Fayemi, O.E.; Sherif, E.-S.M.; et al. Electrochemical evaluation of Cd2+ and Hg2+ ions in water using ZnO/Cu2ONPs/PANI modified SPCE electrode. *Sens. Bio-Sens. Res.* **2022**, *35*, 100476.
10. Lata, S.; Ansari, N.G. Analytical Techniques for Heavy Metal Analysis. In *Heavy Metal Contamination in the Environment*; CRC Press: Boca Raton, FL, USA, 2024; pp. 180–202.
11. Workman, J., Jr. Exploring the Spectrum of Analytical Techniques for Material Characterization. *Spectroscopy* **2023**, 38, 6–13.
12. Okpara, E.C.; Fayemi, O.E.; Wojuola, O.B.; et al. Electrochemical detection of selected heavy metals in water: A case study of African experiences. *RSC Adv.* **2022**, *12*, 26319–26361.
13. Pasakon, P.; Kamsong, W.; Primpray, V.; et al. Simultaneous electrochemical sensing of Cd^{2+} and Pb^{2+} using screen-printed ionic liquid/graphene electrodes. *Int. J. Environ. Anal. Chem.* **2024**, *104*, 9804–9819.
14. Waheed, A.; Mansha, M.; Ullah, N. Nanomaterials-based electrochemical detection of heavy metals in water: Current status, challenges and future direction. *TrAC Trends Anal. Chem.* **2018**, *105*, 37–51.
15. Brownson, D.A.; Banks, C.E. Graphene electrochemistry: An overview of potential applications. *Analyst* **2010**, *135*, 2768–2778.
16. Pumera, M. Electrochemistry of graphene: New horizons for sensing and energy storage. *Chem. Rec.* **2009**, *9*, 211–223.
17. Brownson, D.A.; Kelly, P.J.; Banks, C.E. In situ electrochemical characterisation of graphene and various carbon-based electrode materials: An internal standard approach. *RSC Adv.* **2015**, *5*, 37281–37286.
18. McCreery, R.L. Advanced carbon electrode materials for molecular electrochemistry. *Chem. Rev.* **2008**, *108*, 2646–2687.
19. Aragay, G.; Pons, J.; Merkoçi, A. Enhanced electrochemical detection of heavy metals at heated graphite nanoparticle-based screen-printed electrodes. *J. Mater. Chem.* **2011**, *21*, 4326–4331.
20. Somerset, V.; Iwuoha, E.; Hernandez, L. Stripping voltammetric measurement of trace metal ions at screen-printed carbon and carbon paste electrodes. *Procedia Chem.* **2009**, *1*, 1279–1282.
21. Somerset, V.; Leaner, J.; Mason, R.; et al. Development and application of a poly (2,2′-dithiodianiline)(PDTDA)-coated screen-printed carbon electrode in inorganic mercury determination. *Electrochim. Acta* **2010**, *55*, 4240–4246.
22. Ferrari, A.G.-M.; Carrington, P.; Rowley-Neale, S.J.; et al. Recent advances in portable heavy metal electrochemical sensing platforms. *Environ. Sci. Water Res. Technol.* **2020**, *6*, 2676–2690.
23. Lu, Y.; Ganguli, R.; Drewien, C.A.; et al. Continuous formation of supported cubic and hexagonal mesoporous films by sol–gel dip-coating. *Nature* **1997**, *389*, 364–368.

24. Petit-Dominguez, M.D.; Shen, H.; Heineman, W.R.; et al. Electrochemical behavior of graphite electrodes modified by spin-coating with sol−gel-entrapped ionomers. *Anal. Chem.* **1997**, *69*, 703–710.
25. Kim, Y.-R.; Bong, S.; Kang, Y.-J.; et al. Electrochemical detection of dopamine in the presence of ascorbic acid using graphene modified electrodes. *Biosens. Bioelectron.* **2010**, *25*, 2366–2369.
26. Lu, Y.; Liang, X.; Niyungeko, C.; et al. A review of the identification and detection of heavy metal ions in the environment by voltammetry. *Talanta* **2018**, *178*, 324–338.
27. Somasundrum, M.; Bannister, J.V. Amperometric determination of copper using screen-printed electrodes. *Sens. Actuators B Chem.* **1993**, *15*, 203–208.
28. Kadara, R.O.; Jenkinson, N.; Banks, C.E. Disposable bismuth oxide screen printed electrodes for the high throughput screening of heavy metals. *Electroanal. Int. J. Devoted Fundam. Pract. Asp. Electroanal.* **2009**, *21*, 2410–2414.
29. Palchetti, I.; Upjohn, C.; Turner, A.; et al. Disposable screen-printed electrodes (SPE) mercury-free for lead detection. *Anal. Lett.* **2000**, *33*, 1231–1246.
30. Kadara, R.O.; Tothill, I.E. Development of disposable bulk-modified screen-printed electrode based on bismuth oxide for stripping chronopotentiometric analysis of lead (II) and cadmium (II) in soil and water samples. *Anal. Chim. Acta* **2008**, *623*, 76–81.
31. Alagumalai, K.; Sivakumar, M.; Kim, S.-C.; et al. $AgBiS_2$ embedded activated graphene nanolayer for sensing azathioprine in biospecimens. *Colloids Surf. A Physicochem. Eng. Asp.* **2024**, *685*, 133243.
32. Hamad, A.; Khashan, K.S.; Hadi, A. Silver nanoparticles and silver ions as potential antibacterial agents. *J. Inorg. Organomet. Polym. Mater.* **2020**, *30*, 4811–4828.
33. Gan, X.; Liu, T.; Zhong, J.; et al. Effect of silver nanoparticles on the electron transfer reactivity and the catalytic activity of myoglobin. *ChemBioChem* **2004**, *5*, 1686–1691.
34. Zahran, M.; Khalifa, Z.; Zahran, M.A.-H.; et al. Recent advances in silver nanoparticle-based electrochemical sensors for determining organic pollutants in water: A review. *Mater. Adv.* **2021**, *2*, 7350–7365.
35. Ivanišević, I. The role of silver nanoparticles in electrochemical sensors for aquatic environmental analysis. *Sensors* **2023**, *23*, 3692.
36. Wang, J. Stripping analysis at bismuth electrodes: A review. *Electroanal. Int. J. Devoted Fundam. Pract. Asp. Electroanal.* **2005**, *17*, 1341–1346.
37. Wang, J.; Lu, J.; Hocevar, S.B.; et al. Bismuth-coated carbon electrodes for anodic stripping voltammetry. *Anal. Chem.* **2000**, *72*, 3218–3222.
38. Chang, J.; Li, Y.; Duan, F.; et al. Selective removal of chloride ions by bismuth electrode in capacitive deionization. *Sep. Purif. Technol.* **2020**, *240*, 116600.
39. Kokkinos, C.; Economou, A. Stripping analysis at bismuth-based electrodes. *Curr. Anal. Chem.* **2008**, *4*, 183–190.
40. Krueger, J.; Winkler, P.; Luderitz, E.; et al. Bismuth Alloys and Bismuth Compounds. *Ullman Encycl. Ind. Technol.* **1978**, *3*.
41. Miao, Y.; Wang, Z.; Wei, Z.; et al. Patterned growth of AgBiS 2 nanostructures on arbitrary substrates for broadband and eco-friendly optoelectronic sensing. *Nanoscale* **2024**, *16*, 7409–7418.
42. Hu, L.; Patterson, R.J.; Zhang, Z.; et al. Enhanced optoelectronic performance in AgBiS 2 nanocrystals obtained via an improved amine-based synthesis route. *J. Mater. Chem. C* **2018**, *6*, 731–737.
43. Senina, A.; Prudnikau, A.; Wrzesińska-Lashkova, A.; et al. Cation exchange synthesis of AgBiS 2 quantum dots for highly efficient solar cells. *Nanoscale* **2024**, *16*, 9325–9334.
44. Gopi, P.K.; Sanjayan, C.G.; Akhil, S.; et al. Silver bismuth sulphide (AgBiS2)-MXene composite as high-performance electrochemical sensing platform for sensitive detection of pollutant 4-nitrophenol. *Electrochim. Acta* **2024**, *498*, 144616. https://doi.org/10.1016/j.electacta.2024.144616.
45. Li, R.; Wang, C.; Wang, Y.; et al. A novel photoelectrochemical sensor based on flower-like SnS_2, sea urchin-like AgBiS2 and graphene oxide nanocomposite film for efficient and sensitive detection of acetaminophen in lake water samples. *Anal. Chim. Acta* **2023**, *1239*, 340681. https://doi.org/10.1016/j.aca.2022.340681.
46. Ajiboye, T.O.; Oyewo, O.A.; Marzouki, R.; et al. Synthesis of AgBiS2/gC3N4 and its application in the photocatalytic reduction of Pb(II) in the matrix of methyl orange, crystal violet, and methylene blue dyes. *Ceram. Int.* **2023**, *49*, 6149–6163. https://doi.org/10.1016/j.ceramint.2022.10.187.
47. Olowu, R.A.; Ndangili, P.M.; Baleg, A.A.; et al. Spectroelectrochemical dynamics of dendritic poly (propylene imine)-polythiophene star copolymer aptameric 17β-estradiol biosensor. *Int. J. Electrochem. Sci.* **2011**, *6*, 1686–1708.
48. Honeychurch, K.C.; Hart, J.P.; Cowell, D.C. Voltammetric Behavior and Trace Determination of Lead at a Mercury-Free Screen-Printed Carbon Electrode. *Electroanal. Int. J. Devoted Fundam. Pract. Asp. Electroanal.* **2000**, *12*, 171–177.
49. Okpara, E.C.; Nde, S.C.; Fayemi, O.E.; et al. Electrochemical characterization and detection of lead in water using SPCE modified with BiONPs/PANI. *Nanomaterials* **2021**, *11*, 1294.

50. Mariappan, C.; Roling, B. Investigation of bioglass–electrode interfaces after thermal poling. *Solid State Ion.* **2008**, *179*, 671–677.
51. Rani, G.; Rajesh Banu, J.; Yogalakshmi, K.N. Chapter 18-Electrode modification and its application in microbial electrolysis cell. In *Scaling Up of Microbial Electrochemical Systems*; Jadhav, D.A., Pandit, S., Gajalakshmi, S., et al., Eds.; Elsevier: Amsterdam, The Netherlands, 2022; pp. 339–357.
52. Macdonald, J.R.; Johnson, W.B.; Raistrick, I.; et al. *Impedance Spectroscopy: Theory, Experiment, and Applications*; John Wiley & Sons: Hoboken, NJ, USA, 2018.
53. Laschuk, N.O.; Easton, E.B.; Zenkina, O.V. Reducing the resistance for the use of electrochemical impedance spectroscopy analysis in materials chemistry. *RSC Adv.* **2021**, *11*, 27925–27936.
54. Pérez-Ràfols, C.; Bastos-Arrieta, J.; Serrano, N.; et al. Ag Nanoparticles Drop-Casting Modification of Screen-Printed Electrodes for the Simultaneous Voltammetric Determination of Cu(II) and Pb(II). *Sensors* **2017**, *17*, 1458.
55. Guyett, P.C.; Chew, D.; Azevedo, V.; et al. Optimizing SEM-EDX for fast, high-quality and non-destructive elemental analysis of glass. *J. Anal. At. Spectrom.* **2024**, *39*, 2565–2579.
56. Shirley, B.; Jarochowska, E. Chemical characterisation is rough: The impact of topography and measurement parameters on energy-dispersive X-ray spectroscopy in biominerals. *Facies* **2022**, *68*, 7. https://doi.org/10.1007/s10347-022-00645-4.
57. Yedra, L.; Kumar, C.S.; Pshenova, A.; et al. A correlative method to quantitatively image trace concentrations of elements by combined SIMS-EDX analysis. *J. Anal. At. Spectrom.* **2021**, *36*, 56–63.
58. Lifshin, E.; Gauvin, R. Precision and detection limits for EDS analysis in the SEM. *Microsc. Today* **2003**, *11*, 46–49.
59. Ajiboye, T.O.; Mafolasire, A.A.; Lawrence, S.; et al. Composite and Pristine Silver Bismuth Sulphide: Synthesis and Up-to-Date Applications. *J. Inorg. Organomet. Polym. Mater.* **2024**, *34*, 433–457.
60. Kreider-Mueller, A.; Quinlivan, P.J.; Owen, J.S.; et al. Tris (2-mercaptoimidazolyl) hydroborato cadmium thiolate complexes,[TmBut] CdSAr: Thiolate exchange at cadmium in a sulfur-rich coordination environment. *Inorg. Chem.* **2017**, *56*, 4643–4653.
61. Semenov, V.N.; Naumov, A.V.; Samofalova, T.V.; et al. The deposition of layers of sulfides of cadmium and lead from thiosulfate-tiourea complexes and their properties. *Kondens. Sredy I Mezhfaznye Granitsy = Condens. Matter Interphases* **2019**, *21*, 240–248.
62. Saha, D.; Barakat, S.; Van Bramer, S.E.; et al. Noncompetitive and competitive adsorption of heavy metals in sulfur-functionalized ordered mesoporous carbon. *ACS Appl. Mater. Interfaces* **2016**, *8*, 34132–34142.
63. Yang, Q.; Sun, X.; Sun, Y.; et al. Bismuth metal–organic framework/carbon nanosphere composites for ultrasensitive simultaneous electrochemical detection of lead and cadmium. *ACS Appl. Nano Mater.* **2023**, *6*, 7901–7909.
64. Wu, Y.; Li, N.B.; Luo, H.Q. Simultaneous measurement of Pb, Cd and Zn using differential pulse anodic stripping voltammetry at a bismuth/poly (p-aminobenzene sulfonic acid) film electrode. *Sens. Actuators B Chem.* **2008**, *133*, 677–681.
65. Li, Z.; Han, H.; Chao, L.; et al. Recent Advances of $AgBiS_2$: Synthesis Methods, Photovoltaic Device, Photodetector, and Sensors. *Electromagn. Sci.* **2025**, *3*, 0090451–1–0090451-19.
66. Ciblak, A.; Mao, X.; Padilla, I.; et al. Electrode effects on temporal changes in electrolyte pH and redox potential for water treatment. *J. Environ. Sci. Health Part A* **2012**, *47*, 718–726.
67. Li, L.-Z.; Yu, S.-Y.; Peijnenburg, W.J.; et al. Determining the fluxes of ions (Pb^{2+}, Cu^{2+} and Cd^{2+}) at the root surface of wetland plants using the scanning ion-selective electrode technique. *Plant Soil* **2017**, *414*, 1–12.
68. Yang, D.; Wang, L.; Chen, Z.; et al. Anodic stripping voltammetric determination of traces of Pb (II) and Cd (II) using a glassy carbon electrode modified with bismuth nanoparticles. *Microchim. Acta* **2014**, *181*, 1199–1206.
69. Laschi, S.; Palchetti, I.; Mascini, M. Gold-based screen-printed sensor for detection of trace lead. *Sens. Actuators B Chem.* **2006**, *114*, 460–465.
70. Bernalte, E.; Arévalo, S.; Pérez-Taborda, J.; et al. Rapid and on-site simultaneous electrochemical detection of copper, lead and mercury in the Amazon river. *Sens. Actuators B Chem.* **2020**, *307*, 127620.
71. Bernalte, E.; Sánchez, C.M.; Gil, E.P. Determination of mercury in ambient water samples by anodic stripping voltammetry on screen-printed gold electrodes. *Anal. Chim. Acta* **2011**, *689*, 60–64.
72. Inman, D.; Sethi, R.; Spencer, R. The effects of complex ion formation and ionic adsorption on electrode reactions involving metals and metal ions in fused salts. *J. Electroanal. Chem. Interfacial Electrochem.* **1971**, *29*, 137–147.
73. Abbas, A.; Amin, H.M. Silver nanoparticles modified electrodes for electroanalysis: An updated review and a perspective. *Microchem. J.* **2022**, *175*, 107166.
74. Furey, A.; Moriarty, M.; Bane, V.; et al. Ion suppression; a critical review on causes, evaluation, prevention and applications. *Talanta* **2013**, *115*, 104–122.
75. Lu, M.; Deng, Y.; Luo, Y.; et al. Graphene aerogel–metal–organic framework-based electrochemical method for simultaneous detection of multiple heavy-metal ions. *Anal. Chem.* **2018**, *91*, 888–895.

76. Awual, M.R.; Khraisheh, M.; Alharthi, N.H.; et al. Efficient detection and adsorption of cadmium(II) ions using innovative nano-composite materials. *Chem. Eng. J.* **2018**, *343*, 118–127. https://doi.org/10.1016/j.cej.2018.02.116.
77. Kim, H.; Boulogne, F.; Um, E.; et al. Controlled uniform coating from the interplay of Marangoni flows and surface-adsorbed macromolecules. *Phys. Rev. Lett.* **2016**, *116*, 124501.
78. Papadas, I.T.; Savva, A.; Ioakeimidis, A.; et al. Employing surfactant-assisted hydrothermal synthesis to control $CuGaO_2$ nanoparticle formation and improved carrier selectivity of perovskite solar cells. *Mater. Today Energy* **2018**, *8*, 57–64.
79. Sochr, J.; Machková, M.; Machynak, L.; et al. Heavy metals determination using various in situ bismuth film modified carbon-based electrodes. *Acta Chim. Slovaca* **2016**, *9*, 28.
80. Xie, T.; Zhang, M.; Chen, P.; et al. A facile molecularly imprinted electrochemical sensor based on graphene: Application to the selective determination of thiamethoxam in grain. *Rsc Adv.* **2017**, *7*, 38884–38894.
81. Fumagalli, D.; Aidli, W.; Falciola, L.; et al. Bimodal (Photo) electrochemical Sensor for Cetirizine Detection. *Electroanalysis* **2025**, *37*, e12018.
82. Maity, S.; Deshmukh, S.; Roy, S.S.; et al. Selenium-doped Graphite for Electrochemical Sensing and Adsorption of Hg (II) and Cd (II) Ions. *ChemElectroChem* **2023**, *10*, e202201044.
83. Blaise, N.; Gomdje Valéry, H.; Maallah, R.; O et al. Simultaneous electrochemical detection of Pb and Cd by carbon paste electrodes modified by activated clay. *J. Anal. Methods Chem.* **2022**, *2022*, 6900839.
84. Zhang, W.; Chen, J.; Xiao, G.; et al. A hydrogel electrochemical electrode for simultaneous measurement of cadmium ions and lead ions. *J. Electroanal. Chem.* **2021**, *901*, 115756.
85. Liu, L.; Yu, C.; Zhang, X.; et al. Carbon paste electrode modified with bismuth oxychloride as a sensor for the determination of Pb^{2+} and Cd^{2+}. *Int. J. Electrochem. Sci.* **2019**, *14*, 4469–4482.
86. Bindewald, E.H.; Schibelbain, A.F.; Papi, M.A.; et al. Design of a new nanocomposite between bismuth nanoparticles and graphene oxide for development of electrochemical sensors. *Mater. Sci. Eng. C* **2017**, *79*, 262–269.
87. Koirala, K.; Santos, J.H.; Tan, A.L.; et al. Chemically modified carbon paste electrode for the detection of lead, cadmium and zinc ions. *Sens. Rev.* **2016**, *36*, 339–346.
88. Shalaby, E.; Beltagi, A.; Hathoot, A.; et al. Simultaneous voltammetric sensing of Zn^{2+}, Cd^{2+}, and Pb^{2+} using an electrodeposited Bi–Sb nanocomposite modified carbon paste electrode. *RSC Adv.* **2023**, *13*, 7118–7128.